

## **Rammed earth as bi-modulus material: experimental and analytical investigations through Euler-Bernoulli and Timoshenko beam models**

---

Giulia Misseri\* and Luisa Rovero

Department of Architecture,  
University of Florence,  
Florence 50121, Italy  
Email: giulia.misseri@unifi.it  
Email: luisa.rovero@unifi.it  
\*Corresponding author

**Abstract:** An experimental campaign aimed at defining mechanical parameters of rammed earth is reported. Compressive strength, Young's modulus and Poisson's coefficient are determined on prismatic specimens. Indirect tension tests and three-point bending tests are carried out as well. The size and shape of specimens are accurately controlled to gain consistent results among tests. Interpretation of test results assumes that rammed earth material has two Young's moduli, in tension and compression. In this framework, closed-form solutions for displacements and position of the neutral axis are properly derived from expressions of the displacement field assuming both Euler-Bernoulli and Timoshenko beam models, and hence retrieving the value of Young's modulus in tension. Results show that the assumption of bi-modulus material provides estimations of longitudinal stress reached during three-point bending tests as consistent with compression and split tests. Also, the Timoshenko model provides slightly less conservative estimations of Young's modulus in tension.

**Keywords:** rammed earth; adobe; bi-modulus model; mechanical tests.

**Reference** to this paper should be made as follows: Misseri, G. and Rovero, L. (2022) 'Rammed earth as bi-modulus material: experimental and analytical investigations through Euler-Bernoulli and Timoshenko beam models', *Int. J. Masonry Research and Innovation*, Vol. 7, No. 5, pp.482–503.

**Biographical notes:** Giulia Misseri received her PhD in Structures and Restoration of Architecture and the Cultural Heritage from the University of Florence in 2017. She is currently an Assistant Professor at the University of Florence. Her research interests include statics and dynamics of masonry structures, fracture mechanics and experimental testing.

Luisa Rovero is an Associate Professor of Structural Mechanics at the Department of Architecture, University of Florence. She is a member of the Committee of the PhD Curriculum Structures and Restoration of Architecture and the Cultural Heritage of PhD in Architecture of the University of

Florence. Her current research activity is mainly focused on mechanical behaviour of masonry structures, analysis and modelling of fibre-reinforced inorganic matrix materials for the reinforcement of masonry structures.

---

## 1 Introduction

Collecting soil and arranging it into to erect a shelter against external environment is as ancient as human being and widespread all over the world under kaleidoscopic changeable forms. A third of global population, roughly two billions of people settled in more than 150 countries, lives or works in earthen buildings, homogeneously diffused at every latitude with very adaptable shapes, from poor settlements to monumental heritage or contemporary architectures (Houben and Guillaud, 1994; Fratini et al., 2011; Rovero and Tonietti, 2012; Gamrani et al., 2012; Rovero et al., 2009; Rovero and Tonietti, 2014; Rovero et al., 2020; Boostani et al., 2018; Azil et al., 2020; Liberotti et al., 2016; Fratini et al., 2015). Over 10% of the World Heritage properties incorporate earthen structures. CRAterre (International Centre on Earthen Architecture) reports that raw earth remains today the most widespread building material all around the world. The main resource employed, raw earth, is intrinsically non-polluting and buildings based on it can provide liveable micro-climates in extremely warm contexts due to the good thermal and acoustic isolation properties. Earth is the most affordable resource to build with, and as a result, employing it extensively can contribute to poverty alleviation and sustainable development (UNESCO, 2017). According to the Scopus research database, investigations of earthen-based building materials and technologies has increased markedly in the last two decades; just journal articles pass from a few per year to several tens, only as far as concerns engineering, material and environmental sciences. Among the most debated issues, there are mechanical behaviour, e.g., compressive strength determination and soil selection, structural response against seismic loads, durability and thermal conductivity of earth.

Despite the several advantages, earthen material can in fact exhibit undesirable drawbacks such as reduced mechanical capacity compared to other building materials, deterioration due to moisture and weathering erosion (Minke, 2005). Nonetheless, the low-price combined with the high availability and sustainability of this technology suggests how relevant is, on one hand, to implement new earthen buildings, and on the other, to calibrate adequate strengthening methods for the protection of monuments and historical constructions. To these aims, a better understanding of mechanical behaviour is deemed necessary.

Earthen structures can counteract mechanical compressive actions efficaciously when low rise buildings with massive walls are implemented. Tensile forces are by far more dangerous and even moderate earthquakes can cause catastrophic effects, e.g., Langenbach et al. (2005). In historical earthen buildings, seismic vulnerability has been traditionally mitigated employing different techniques, most of them are based on the use of wood elements. Strengthening systems based on the use of wood are widely spread among several building cultures all around the world. These systems are investigated, for example, in Lourenço et al. (2019), Cancino et al. (2014), Briceno et al. (2019), Vissilia and Villi (2010) and Misseri et al. (2020) and also recommended by some standards and self-building codes (IAEE, 2004; NMAC, 1982). Wooden tying systems are considered

beneficial in activating global response of buildings (Ortega et al., 2017). However, specific evaluations are not so widespread. Michiels (2015) catalogues available timber strengthening systems and Ortega et al. (2018) try to interpret their contribution through FEM modelling of a reference building. In Parisi et al. (2019), a timber-reinforced earthen tower is modelled through nonlinear static analysis and macro-element approach.

Lately, natural or synthetic fibre textiles are also considered, in particular the role of natural fibre textile, polypropylene and nylon grids adhered to adobe walls through earthen mortar is the object of long-term investigation (Blondet et al., 2019, 2008; Blondet and Aguilar, 2007; Portugal and Tarque, 2019; Blondet et al., 2011; Bove et al., 2016; Boostani et al., 2020).

A few national codes consider earthen buildings and related design rules (NSZ, 1998; NMAC, 1982), also for those classified as cultural heritage (INN, 2013); reviews of available national standards aimed at safety of earthen structures and selection of soils are reported in Cid et al. (2011) and Jiménez Delgado and Guerrero (2007) respectively.

Whereas, standards for characterisation of mechanical properties of earth-based materials are still not available; efforts on this are put by RILEM TC 274 (Fabbri et al., 2018). Hence, remarkable investigation efforts are aimed at the definition of mechanical characterisation protocols, e.g., Silveira et al. (2013), Rodríguez-Mariscal et al. (2018) and Illampas et al. (2014) and references reported therein. The main debated issues concern composition and pre-treatment of raw soil, size and shape of specimens, testing procedures and instrumentation layout. In Silveira et al. (2013), a compression and split tests on cylindrical specimens are carried out on existing adobe blocks. Indeed, making cylindrical cores from bricks sampled on site can be more viable than cutting out prisms. Also, cylindrical specimens are preferred since this shape can avoid disturbance in stress distribution that can arise with sharp edges, although installation of deformation sensors might not be straightforward. However, it is not infrequent that whole adobe blocks are tested to retrieve compressive strength, resulting in an unavoidable overestimations due to the confinement effect. As highlighted by Morel et al. (2007), correction factors for compressive strength depending on aspect ratio available for fired bricks can be employed, but may not be suitable for stocky earth blocks. Illampas et al. (2014) provide a detailed review of possible specimen shapes, dimensions and ratios available in the recent literature. As a result of such a variability, Illampas et al. (2014) remark that it is not always possible to compare results of different experimental campaigns, which provide values of compressive strength ranging between 0.6 MPa to 8.3 MPa, although the most common values belong to the range 0.8 MPa–3.5 MPa. Concerning specimen instrumentation, Rodríguez-Mariscal et al. (2018) confirm that strains measured through reading of the testing machine, instead of displacement sensors, may lead to erroneous estimations of the Young's modulus.

In addition to uniaxial compression tests, indirect tension and three point bending tests are often exploited to correlate mechanical properties and estimate flexural and tensile properties. In the indirect tension test, a cylinder or a square prism is compressed through two thin bars made of steel placed on opposing faces. This causes the block to split along the plane of load. The test is conceived for hardened concrete (EN-12390-6, 2009), and the elastic solution to the Flamant-Boussinesq problem is adjusted to retrieve failure stress. In the three point bending test, the specimen is subjected to a single point force up to failure. International standards aimed at hardened mortar testing (EN-1015-11, 2019), recommend to evaluate flexural stress through the Navier solution

of a bent Euler-Bernoulli beam subjected to a point-force; hence, it is assumed that the tested material behaves symmetrically in tension and compression.

In Caporale et al. (2014a, 2014b) and Parisi et al. (2015), the bi-modulus model is applied to earthen material. Already in the studies by de Saint-Venant (1864), it was recognised that some materials can exhibit different elastic behaviour when tightened or compressed. Bending of beams not following Hooke's law is considered by Timoshenko and Goodier (1930), who provide, through equilibrium considerations, the shifted position for neutral axis. Effective modulus of stiffness for pure bending is then provided by Marin (1962). Ambartsumyan (1695) rediscovers the idea of bi-modulus materials and broaden the model to two-dimensions; applications concern fibre-reinforced composites, which exhibit relevantly different behaviour depending on the material-coordinate system (Reddy, 2004). Modified constitutive models based on the signs of principal stress or strain are found in Jones (1997), Bert (1977) and Tran and Bert (1982) and references reported therein.

Provided the discontinuity in the constitutive law due to material bi-modularity, very few problems can be solved analytically and dedicated iterative algorithms must be calibrated to solve general-loading plane-stress problems. Yao and Ye (2004a, 2004b) employ the beam model for pure bending and lateral force bending. He et al. (2009) focus on fast iterative solutions to plane stress problems assuming a constitutive model for which elasticity constants depend on the signs of principal stresses; a similar approach is employed by Zhang et al. (2011, 2016). A detailed review on recent advances is provided in Sun et al. (2010). Furthermore, functionally-graded, bi-modulus materials with unchanged Poisson's ratio are considered in He et al. (2018). No-tension and no-compression materials, which can be regarded as bi-modular, are analysed by Kanno (2011) employing tools of convex analysis. Variational principles, which make use of internal variables to characterise the tensions/compression state, have been defined as well in Du and Guo (2014) and Du et al. (2016).

Recent experimental investigations confirm that the asymmetry of positive and negative stress-strain relations is typical of both organic and inorganic materials, such as concrete, ceramics (Mattos et al., 1992), graphite (Liu et al., 1998), and biological materials (Janmey et al., 2007; Rosakis et al., 2015). Tests on brittle materials such as concrete made of quartzite and Portland cement demonstrate that compression modulus can range up to three times that in tension (Du et al., 2016). This can be also the case of raw earth. In Parisi et al. (2015), a wide experimental campaign on adobe bricks is reported and bi-modulus material assumption is employed to interpret tests. In Caporale et al. (2014a, 2014b, 2015), experimental results are employed and effects of bi-modulus assumption are assessed through FEM micro-mechanical analysis.

In this study, the experimental campaign reported in Section 2 encompasses uniaxial compression tests, indirect tension tests and three-point bending tests on specimens created for the purpose. Then, interpretation of the mechanical behaviour of specimens subjected to three-point bending tests is carried out assuming compacted earth as a bi-modulus material. Differently from previous studies, here, solution to the equilibrium problem is obtained stemming from the displacement field equations. Then, enforcing compatibility and constitutive behaviour enables to solve equilibrium and retrieve displacement equations. Both Euler-Bernoulli and Timoshenko beam models are employed with the aim of incorporating also the shearing effect on the deflection due to the reduced slenderness of specimens subjected to this test. Analytical investigation is reported at the beginning of Section 3. Application of the analytical model to the

experimental outcomes is reported later on in the same section. Discussion on results and conclusions are drawn at the end of the paper.

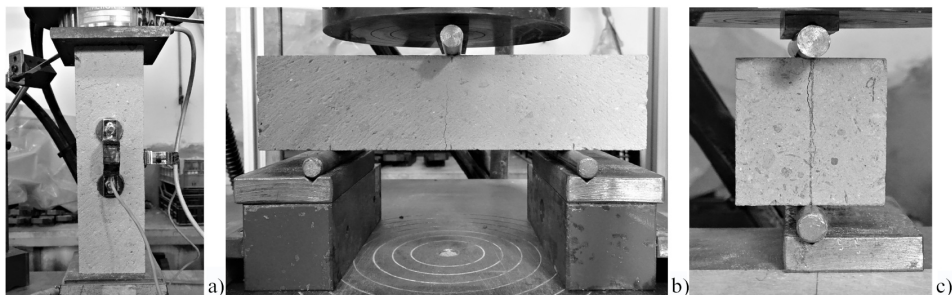
## 2 Materials and methods

### 2.1 Specimens and tests

Raw earth employed to produce specimens has been collected on a selected site in the nearby of a little town called Terranuova Bracciolini in Tuscany, Italy, where earthen constructions used to be traditional. The collected raw earth was air-dried in a controlled environment so as to reach homogeneous relative humidity. Then, cleaning and grinding phases permitted to reach a raw material homogeneous at sight. Vegetal inclusions and little stone chips had to be removed, so sifting was carried out employing a set of standard sieves with looser mesh equal to 2 mm. After having reached a controlled size, earth was dried for 24 hrs in an electric ventilated oven at 60°C.

To fabricate the earth slurry, a controlled quantity of water was added to the dusty soil. Earth was weighted after the drying phase and 11% ratio of water was added so as to reach adequate workability of the slurry, based on the results of several variations of water percentage. Mixing earth and water was carried out with an electric mixer kept at low speed so as to make a slurry as homogenous as possible. For each batch, mixing was controlled in time, five minutes were considered enough for water to accommodate among grains. After these phases, the slurry was casted into the moulds and adjusted manually by applying gentle pressure. After 48 hours, specimens were de-moulded and left drying in controlled environment, i.e., 20°C temperature and 40% relative humidity, for at least 28 days.

**Figure 1** Reference specimens undergoing, (a) uniaxial compression test, where omega shaped extensometers and displacement transducers are clearly visible  
(b) three-point bending test (c) indirect tension test



After the curing time, specimens were measured in terms of volume and weight. The apparent bulk density was evaluated; the average value obtained is  $\gamma = 1.951 \text{ g/cm}^3$  (with coefficient of variation  $\text{CoV} = 0.014$ ). The raw earth employed for specimens was subjected also to granulometry test after the curing phase. The grain size distribution has been carried out through sieving in order to separate the following fractions: sand ( $\phi > 63 \mu\text{m}$ ), silt ( $4 \mu\text{m} < \phi < 63 \mu\text{m}$ ) and clay ( $\phi < 4 \mu\text{m}$ ). Two specimens, RE-1 and RE-2, of 11.7 g and 10.7 g respectively were analysed. Results show a silty sand for

the composition. In particular, for RE-1, it is found 53% of sand, 28% of silt and 19% clay. For RE-2 proportions are 55% sand, silt 27% and clay 18%.

Samples subjected to mechanical tests were labelled according to two alphanumeric codes, XX-YY. The first code stands for test type (XX-), the second code is the progressive number of specimen (YY). The tests carried out and the related samples are:

- *Uniaxial compression (UC)* to determine Young's modulus, compressive strength and Poisson's coefficient. One sample made of eight prismatic specimens, ( $a \times a \times H$ ), with labels UC-YY and nominal dimensions  $60 \times 60 \times 210$  mm was prepared.
- *Three-point bending (TB)* to determine maximum deflection and stress. One sample made of 6 prismatic specimens, ( $a \times a \times L$ ), labelled TB-YY and with nominal dimensions  $60 \times 60 \times 240$  mm was prepared.
- *Indirect tension test (IT)* to estimate tensile strength. One sample made of 13 cubic specimens, ( $a \times a \times a$ ), with labels IT-YY and nominal dimensions  $60 \times 60 \times 60$  mm.

Load rate for tests were adjusted based on the available standards on other materials, basically hardened mortar and concrete. The common framework considered was to keep the test as smooth as possible and, at the same time, to possibly reach failure of the specimens in no more than 120 s. All the tests were carried out employing a 50 KN load cell (TCLP-5B, Tokyo Sokki Kenkyujo C. Ltd). For uniaxial compression tests, a load rate of 100 N/s was employed so that failure occurred in the range 65 s–115 s. For three-point bending tests, the load rate equal to 10 N/s was set, so that failure occurred in the range 75 s–120 s. For indirect tension tests, the load rate equal to 20 N/s was set so that failure occurred in 80 s–100 s. All the tests were carried out in displacement control so as to follow the equilibrium path also after the peak load was reached.

Concerning instrumentation and measurements, the global displacement parameter, i.e., in the direction of the applied load, was recorded directly by the test press. Moreover, for the uniaxial compression tests two 50 mm omega-shaped extensometers were placed at mid height to record strains in the direction of load and along the orthogonal one, see Figure 1(a). Two cantilever displacement transducers were placed over the upper steel plate transmitting load so as to control any asymmetry during tests. The load was applied monotonically up to failure for all tests and the tangent Young's modulus was evaluated at one third of the compressive strength recorded, in agreement with Rodríguez-Mariscal et al. (2018). Monotonic load application was preferred to avoid premature compaction phenomena, microcracking, and consequently development of inelastic strains on unloading branches possibly induced by cyclic loading.

For specimens, a prismatic shape rather than cylindrical was employed for convenience with respect to the available equipment in the laboratory. All the specimens show the same length of the minimum side, i.e., 60 mm. Such a dimension was chosen with the aim of reducing the consequences of possible defects and size of grains, anyway at most equal to 2 mm.

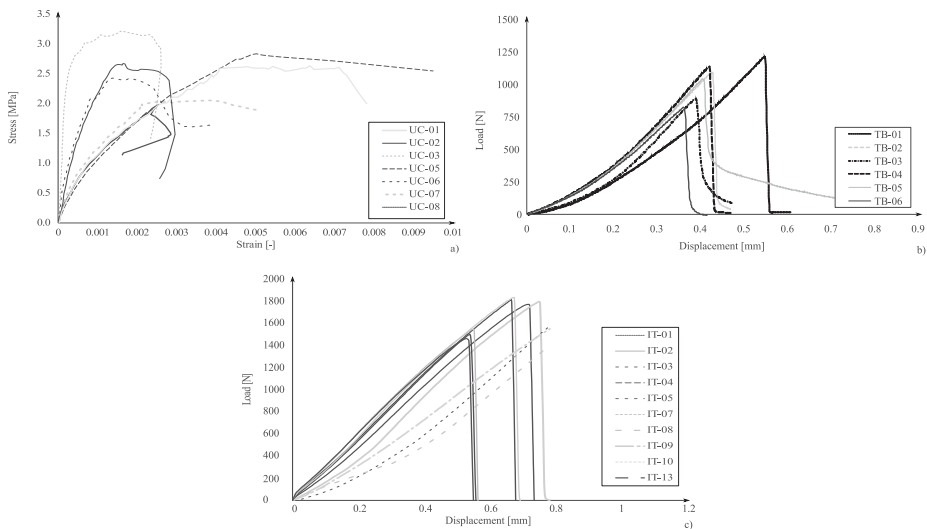
Concerning geometric proportions, for specimens subjected to uniaxial compression tests, nominal dimensions  $a \times a \times H = 60 \times 60 \times 210$  mm, it was considered to provide an edge to height ratio, ( $a/H$ ), higher than to 1/3, so as to assure a sufficiently broad middle third to apply the 50-mm omega shaped extensometers. More slender

specimens might have been considered, but this was avoided due to the possibility of damaging them during test preparation.

For the specimens subjected to three-point bending tests, nominal dimensions  $a \times a \times L = 60 \times 60 \times 240$  mm, the edge to length ratio,  $(a/L)$ , suggested for hardened mortar specimens in EN-1015-11 (2019) and equal to 4 was kept the same. Also, the proportions prisms edge – free span, i.e., distance between supports,  $L_0$ , is equal to  $2/5$ . This is the value suggested in EN-1015-11 (2019) for mortar specimens, hence, in TB sample, edge is  $a = 60$  mm and free span is  $L_0 = 150$  mm.

Concerning the dimensions and proportions of specimens subject to indirect tension tests, it was decided to keep the same cross section dimension of other specimens. Cubic shape of specimens, instead of cylindrical, is employed. Indeed, assuming the cylinder inscribed in the square-base specimen, the compressed circular cross section is loaded by the two antipodal concentrated forces. As a result, tension stress develops in the direction orthogonal to the load.

**Figure 2** Results of, (a) uniaxial compression tests on prismatic specimens (b) three-point bending tests on prismatic specimens classified TB1 (c) indirect tension tests on prismatic specimens



## 2.2 Test results

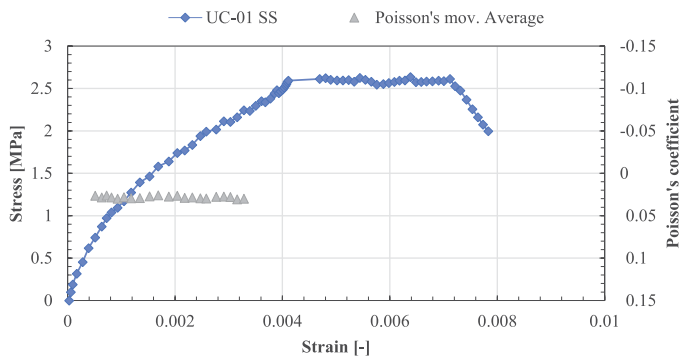
Concerning uniaxial compression tests, results in terms of stress – strain diagrams are reported in Figure 2(a). All the specimens showed a recognisable linear elastic phase up to around half of the maximum load reached. After that point, load increases more slowly and a slightly nonlinear elastic phase commences before reaching the peak. After reaching peak load, softening occurred slowly. The test was considered concluded after having reached 80% of the peak load. Specimens showed sub-vertical cracks in the phase prior to peak, demonstrating a correct execution of the test, see Figure 3. Stress is computed dividing the recorded force over the cross section area. Strain is obtained

directly from the measurements of the vertical extensometer with 50 mm base length. The compressive Young’s modulus was evaluated as the secant modulus at one third of the peak stress.

**Figure 3** Cracked reference specimen subjected to uniaxial compression test



**Figure 4** Stress – strain diagram for specimen UC-01 superposed to the Poisson’s coefficient – strain diagram as per refined by moving average over three values (see online version for colours)



To evaluate the value of Poisson’s coefficient, the records of the two extensometers were employed. The ratio vertical-to-horizontal strains was considered for the records in the linear-elastic phase of the test. In fact, for all specimens, after an initial phase, strain recordings converge to a fairly stable response before peak load. The reference value of the Poisson’s coefficient is evaluated as follows. First, the values of moving average spanning three values are evaluated in the recordings of vertical-to-horizontal strains ratio (multiplied for  $-1$ ), then, the arithmetic average of the moving average values is

computed. The minimum value between the arithmetic average and the value of the coefficient recorded at one third of peak stress, i.e., same point where the compression Young's modulus was evaluated, is picked as the Poisson's coefficient. Figure 4 shows the stress strain diagram for a reference specimen superposed to the correspondent graph of the vertical-to-horizontal strains ratio plotted over vertical strains.

For a sub group of specimens, diagrams appear well clustered and the same quality of the equilibrium path was recorded. For specimens UC-02, UC-06 and UC-07, a stiffer linear elastic branch can be recognised. In particular, for specimen UC-07, which exhibited the stiffest response, also the highest peak stress was reached, while UC-02 and UC-06 are comparable to the others in terms of peak values.

The average peak stress is  $\sigma_c = 2.567$  MPa (st. dev. = 0.412 MPa and coefficient of variation, CoV = 0.161). The average value of Poisson's ratio in compression is  $\nu_c = 0.0449$  (st. dev. = 0.0329 and CoV = 0.73) and average value of Young's modulus is  $E_c = 2,239$  MPa (st. dev. = 1,282 MPa, CoV = 0.57). If the subset of specimens UC-03, UC-04 and UC-05, UC-07 and UC-08, is considered, the average value of the Young's modulus is much more stable,  $E_c = 1,462$  MPa (st. dev. = 292 MPa, CoV = 0.20).

For three-point bending tests, results in terms of load – displacement diagrams are reported in Figure 2(b). All the specimens showed an initial accommodation phase, possibly connected to indentation, and a clear linear elastic trend in a second stage, up to the maximum load reached. Then, load falls abruptly due to the sudden opening of a central vertical crack and the formation of two stumps. Specimens showed a sub-vertical crack in correspondence of the loaded cross section, as showed in Figure 1(b), demonstrating a correct execution of the tests. The average peak load reach is satisfactorily stable,  $W_{\max} = 1,030$  N (st. dev. = 150 N, CoV = 0.145).

Results of the indirect tension tests are showed in Figure 2(c) in terms of load and displacement, as recorded during tests. All the specimens failed exhibiting a clear vertical crack under the steel cylinder of the kind represented in Figure 1(c). The maximum indirect tension stress reached was evaluated as  $\sigma_{it} = 2W_{\max}/(A\pi)$ ; where  $W_{\max}$  is the maximum recorded load and  $A$  is the area of the vertical cross section of the specimen aligned with the loading plane. Experiments provide fairly stable results, with average  $\sigma_{it} = 0.29$  MPa (st. dev. = 0.057 MPa, CoV = 0.197).

### 3 Bi-modulus beam under a point force

#### 3.1 Statement and solution of the equilibrium problem

In this section, the solution, in terms of displacements, for a doubly-supported beam under a point force is evaluated according to Ambartsunyan (1695). In particular, material of the beam is considered isotropic and shows two different Young's moduli:  $E_c$ , when it is compressed, and  $E_t$ , when it is tensioned; the two moduli can be related by means of a coefficient  $n = E_t/E_c$ . Shear moduli and Poisson's coefficient are also different if the cross section of the beam is tensioned or compressed,  $G_c = E_c/2(1 + \nu_c)$  and  $G_t = E_t/2(1 + \nu_t)$ . Given the necessary condition of symmetry in the compliance stress tensor:  $\nu_t/E_t = \nu_c/E_c$ , it follows that  $n = \nu_t/\nu_c$ . The differential problem is stated and solved in closed form stemming from the definition of the pertinent displacement field, and imposing compatibility condition and constitutive relations of the bi-modulus material. Differently from previous models, here, the solution

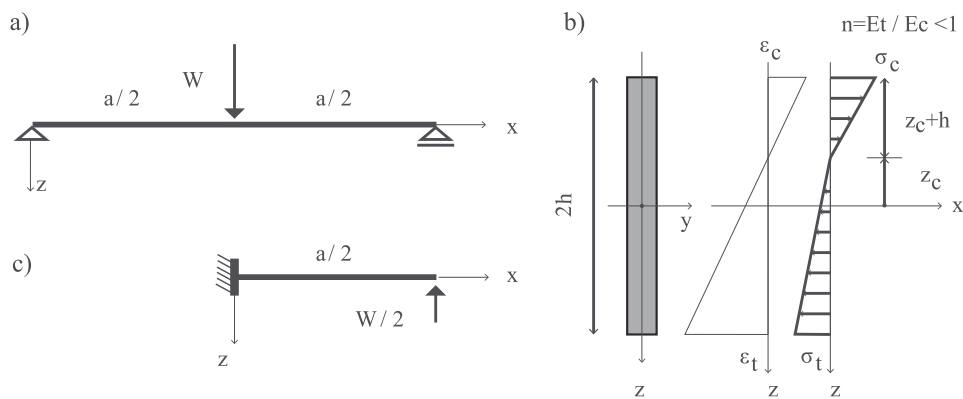
in terms of displacement equations is retrieved for the pin-pin beam loaded by a point force assuming both the Euler-Bernoulli model (EBM) and the Timoshenko model (TM), i.e., accounting for the effect of transverse shear on deflections.

For an orthogonal coordinate system as represented in Figure 5(a), the displacement field for EBM includes displacements components in  $x$ - and  $z$ -directions,  $u(x, z)$  and  $w(x, z)$  respectively, and assumes the following form:

$$\begin{cases} u(x, z) = u_0(x) - z w_{0,x}(x) & (1a) \\ w(x, z) = w_0(x) & (1b) \end{cases}$$

where  $u_0(x)$  and  $w_0(x)$ , are the  $x$ - and  $z$ -direction displacements, respectively, of midline axis; and subscript  $(\cdot)_{,x}$  denotes  $\partial(\cdot)/\partial x$ .

**Figure 5** Scheme of the bent beam assuming a bimodulus material, (a) reference system, dimensions and load case (b) the beam cross section showing asymmetrical strains and discontinuous stress through the height (c) equivalent cantilever beam



For TM, the displacement field includes the displacements components in  $x$ - and  $z$ -directions,  $\tilde{u}(x, z)$  and  $\tilde{w}(x, z)$  respectively, and rotation of transverse normals about the  $x$ -axis,  $\tilde{\psi}(x)$ ; it assumes the following form:

$$\begin{cases} \tilde{u}(x, z) = \tilde{u}_0(x) + z \tilde{\psi}(x) & (2a) \\ \tilde{w}(x, z) = \tilde{w}_0(x) & (2b) \end{cases}$$

where superscript  $\tilde{\cdot}$  employed for displacement functions and any other variable denotes reference to TM. Strain-displacement equations follows directly; for EBM:

$$\begin{cases} \epsilon_{xx}(x) = \epsilon_0(x) + z \epsilon_1(x) = u_{0,x}(x) - z w_{0,xx}(x) & (3a) \\ \gamma_{xz} = 0 & (3b) \end{cases}$$

For TM, it yields:

$$\begin{cases} \tilde{\epsilon}_{xx}(x) = \tilde{\epsilon}_0(x) + z \tilde{\epsilon}_1(x) = \tilde{u}_{0,x}(x) + z \tilde{\psi}_{,x}(x) & (4a) \\ \tilde{\gamma}_{xz}(x) = \tilde{\gamma}_0(x) = \tilde{w}_{0,x}(x) + \tilde{\psi}(x) & (4b) \end{cases}$$

where  $\epsilon_1(x)$  and  $\tilde{\epsilon}_1(x)$  are the part of longitudinal strains due to bending, and varying linearly with  $z$  coordinate. From equation (4b), it is seen that transverse shear strains in TM are constant through the thickness, which can constitute a gross approximation of reality (Reddy, 2004), and identically zero in EBM. Explicating constitutive equations for the isotropic bi-modulus beam it yields for EBM:

$$\sigma_{xx} = \bar{Q}_{11} \left\{ \epsilon_{xx}^{(0)} + z\epsilon_{xx}^{(1)} \right\} \tag{5}$$

$$\tau_{xz} = \bar{Q}_{55} \left\{ \gamma_{xz}^{(0)} \right\} = 0 \tag{6}$$

And for TM:

$$\tilde{\sigma}_{xx} = \bar{Q}_{11} \left\{ \tilde{\epsilon}_{xx}^{(0)} + z\tilde{\epsilon}_{xx}^{(1)} \right\} \tag{7}$$

$$\tilde{\tau}_{xz} = \bar{Q}_{55} \left\{ \tilde{\gamma}_{xz}^{(0)} \right\} \tag{8}$$

where  $\bar{Q}_{ij}$  are the plane-stress-reduced stiffness coefficients (Reddy, 2004, 2006). Resultant forces and moments can be expressed, for the EBM, as:

$$N_{xx} = \int_{-h}^h \sigma_{xx} dz = A \epsilon_0 - B \epsilon_1 \tag{9}$$

$$M_{xz} = \int_{-h}^h \sigma_{xx} z dz = B \epsilon_0 - D \epsilon_1 \tag{10}$$

$$Q_{xz} = M_{xz,x} \tag{11}$$

And for the TM, as:

$$N_{xx} = \int_{-h}^h \sigma_{xx} dz = A \tilde{\epsilon}_0 + B \tilde{\epsilon}_1 \tag{12}$$

$$M_{xz} = \int_{-h}^h \sigma_{xx} z dz = B \tilde{\epsilon}_0 + D \tilde{\epsilon}_1 \tag{13}$$

$$Q_{xz} = \int_{-h}^h \tau_{xz} dz = S \tilde{\gamma}_0 \tag{14}$$

where for both EBM and TM bi-modulus homogeneous beam,  $A$ ,  $B$ ,  $D$  and eventually  $S$  assume the following form:

$$A = \int_{-h}^{z_c} E_c dz + \int_{z_c}^h E_t dz = E_c(h + z_c) + E_t(h - z_c) \tag{15}$$

$$B = \int_{-h}^{z_c} E_c z dz + \int_{z_c}^h E_t z dz = -\frac{1}{2}(E_c - E_t)(h^2 - z_c^2) \tag{16}$$

$$D = \int_{-h}^{z_c} E_c z^2 dz + \int_{z_c}^h E_t z^2 dz = \frac{1}{3}(E_c(h^3 + z_c^3) + E_t(h^3 - z_c^3)) \tag{17}$$

$$S = K^2 \int_{-h}^{z_c} G_c dz + \int_{z_c}^h G_t dz = K^2(G_c(h + z_c) + G_t(h - z_c)) \tag{18}$$

where  $z_c$ , or  $\tilde{z}_c$  in its place if the TM is referred, is the oriented distance of neutral axis, i.e., evaluated from  $z = 0$  towards the compressed part of the cross section, see Figure 5(b), where it is represented the case of  $z_c < 0$ . Then, differential equations of equilibrium for the doubly supported EBM beam are:

$$\begin{cases} N_{xx,x} = 0 & (19a) \\ M_{xz,xx} = 0 & (19b) \end{cases}$$

While for the TM:

$$\begin{cases} N_{xx,x} = 0 & (20a) \\ M_{xz,x} = Q_{xz} & (20b) \\ Q_{xz,x} = 0 & (20c) \end{cases}$$

For EBM, substituting equations (9) and (10) into equation (19) in view of equation (3) yields the following seventh-order system of ODE:

$$\begin{cases} A u_{0,xxx} - B w_{0,xxx} = 0 & (21a) \\ B u_{0,xxx} - D w_{0,xxxx} = 0 & (21b) \end{cases}$$

For TM, substituting equations (12), (13) and (14) into equation (20) in view of equation (4) yields the following sixth-order system of ordinary differential equations (ODE):

$$\begin{cases} A \tilde{u}_{,xx} + B \tilde{\psi}_{,xx} = 0 & (22a) \\ B \tilde{u}_{,xx} + D \tilde{\psi}_{,xx} - S(\tilde{w}_{,x} + \tilde{\psi}) = 0 & (22b) \\ S(\tilde{w}_{,xx} + \tilde{\psi}_{,x}) = 0 & (22c) \end{cases}$$

Considering symmetry of geometry and load, the deflection of the simply supported beam of length  $a$ , subjected to a concentrated force  $W$ , can be investigated considering a cantilever beam clamped in  $x = z = 0$  and free in  $x = a/2$ , subjected to a point force  $W/2$  in  $a/2$ , Figure 5(c).

According to this equivalent geometry layout, for the EBM beam, to solve the system of equation (21), the following seven boundary conditions (BCs) must be satisfied:

$$\begin{cases} u(0) = w(0) = w'(0) = 0 & (23a) \\ M_{xz}(a/2) = N_{xx}(a/2) = 0 & (23b) \\ Q_{xz}(a/2) = -W/2 & (23c) \\ M_{xz}(0) = Wa/4 & (23d) \end{cases}$$

For the TM beam, to solve the system of equation (22), the following six BCs must be satisfied:

$$\begin{cases} \tilde{u}(0) = \tilde{\psi}(0) = \tilde{w}(0) = 0 & (24a) \\ M_{xz}(a/2) = N_{xx}(a/2) = 0 & (24b) \\ Q_{xz}(a/2) = W/2 & (24c) \end{cases}$$

Equations (21) and (23) provide, for the EBM, the following displacement functions:

$$u(x) = -\frac{BWx(x-a)}{4(B^2-AD)} \tag{25}$$

$$w(x) = \frac{AWx^2(3a-2x)}{24(B^2-AD)} \tag{26}$$

Equations (22) and (24) provide, for the TM, the following displacement functions:

$$\tilde{u}(x) = -\frac{BWx(x-a)}{4(B^2-AD)} \tag{27}$$

$$\tilde{w}(x) = \frac{AWx^2(3a-2x)}{24(B^2-AD)} - \frac{Wx}{2S} \tag{28}$$

$$\tilde{\psi}(x) = \frac{AWx(x-a)}{4(B^2-AD)} \tag{29}$$

It is worth noting that  $x$ -direction displacements, equations (25) and (27), are identical for the two models. Transverse,  $z$ -direction, displacement equations, equations (26) and (28), differ in the part that estimate the effect of shearing forces on the beam deflection.

Neutral axis depth can be retrieved imposing that, for  $z = z_c$  or  $z = \tilde{z}_c$ , longitudinal strains, equations (3a) and (4a) for the EBM and TM, respectively, are zero. This yields, for the EBM:

$$z_c = h \left( 1 - \frac{2}{1 + \sqrt{n}} \right) \tag{30}$$

similarly to the results obtained by Timoshenko and Goodier (1930), Yao and Ye (2004a) and Parisi et al. (2015). And for the TM:

$$\tilde{z}_c = \frac{h(1 - 2\sqrt{n} + n)}{n - 1} \tag{31}$$

It is noted that equation (30) is coincident equation (31). Indeed, the TM strain displacement equation (4a) depends on midline stretching,  $\tilde{u}_{0,x}(x)$ , and on the  $x$ -derivative of transverse normal rotations,  $\tilde{\psi}_{,x}(x)$ . Strains depending on midline stretching are identical for the EBM and the TM beam [cf. equations (25) and (27)]. The  $x$ -derivative of transverse normal rotations,  $\tilde{\psi}_{,x}(x)$ , coincides with the opposite of the second derivative of transverse displacements,  $-\tilde{w}_{,xx}(x)$ . In fact, the contribution offered by shear to transverse displacements,  $\tilde{w}(x)$ , equation (28), depends linearly on  $x$ . Hence equation (4a) for  $z = \tilde{z}_c$  offers:

$$\tilde{u}_{0,x}(x) + \tilde{z}_c \tilde{\psi}_{,x}(x) = \tilde{u}_{0,x}(x) - \tilde{z}_c \tilde{w}_{,xx}(x) = 0 \tag{32}$$

which provides equation (31).

Through the analytical model, it is possible to assess the value of longitudinal elasticity modulus in tension, related to the one in compression by means of coefficient  $n$ . Differently from other materials, e.g., fibre composites, for concrete and brittle materials, the coefficient  $n$  tends to take values less than unity. As a result, in a bent beam with upward curvature, e.g., Figure 5(a), cross section turns out to exhibit a wider area subjected to tension than that compressed, and the neutral axis moves away from the most stretched edge Figure 5(b). Hence, for materials that show  $n < 1$ , compression and tension stresses show peak values respectively higher and lower than those obtained through the classic Navier solution.

**Figure 6** For a reference beam  $a = 600$  mm,  $h = 60$  mm, fixed value of load  $W = 1,000$  N, and  $E_c = 30$  GPa, variation in the deflections normalised to span along geometrical axis for varying values of coefficient  $n$  assuming EBM and TM

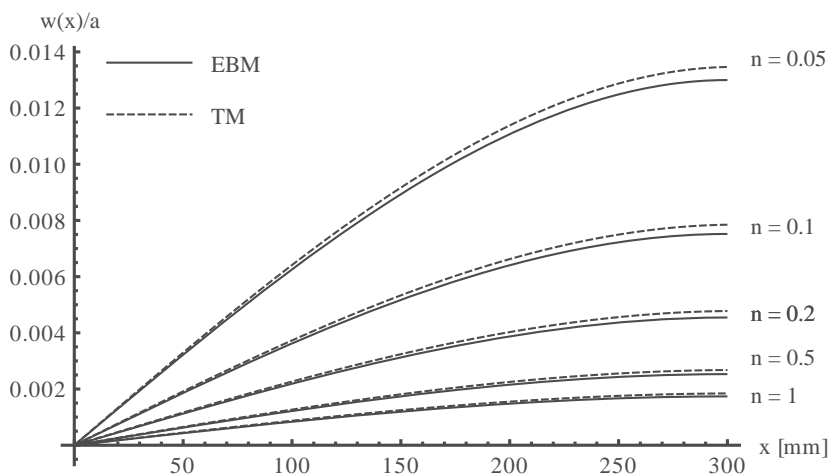
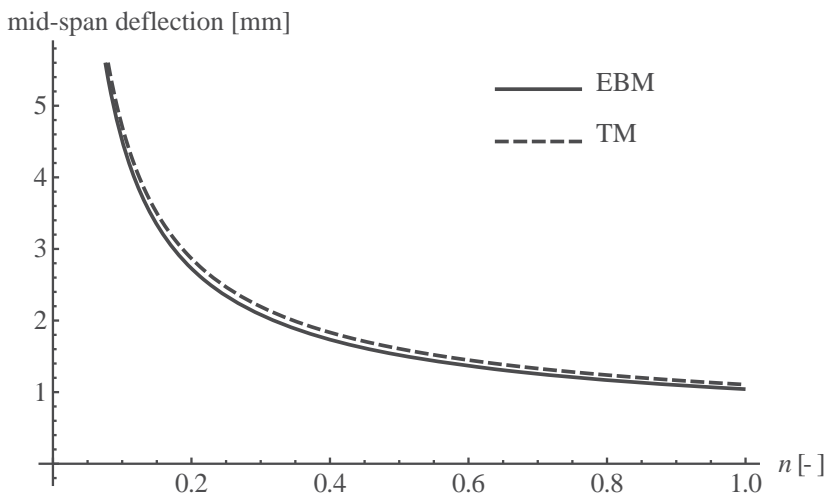


**Figure 7** For the reference specimen, same data of Figure 6, increase in absolute deflection with continuous variation of coefficient  $n$



For a reference case, i.e.,  $a = 600$  mm spanning beam, cross section height  $2h = 120$  mm, loaded by  $W = 1,000$  N and  $E_c = 30$  GPa, Figure 6, shows the diagrams of  $z$ -displacements,  $w(x)$ , normalised with respect to span, i.e.,  $a$ , over position along  $x$  axis. The assumption of bi-modulus material induces remarkable increase in the expected deflections at mid point which passes from around  $1/300$  of the span for  $n = 1$  up to more than three times for low values of  $n$ .

Moreover, concerning predictions provided by the two beam models, it is seen how TM provides more conservative estimations, i.e., higher values of normalised deflection, for decreasing values of the coefficient  $n$ . Specifically, the difference in estimations of normalised deflection at mid-span for the two models passes from  $1/10,000$  of the span with  $n = 1$  to more than  $1/2,000$  of the span for  $n = 0.05$ . These correspond to an absolute mismatch among the two estimates of  $0.063$  mm for  $n = 1$  and  $0.279$  mm for  $n = 0.05$ . Hence, the effect of shearing on deflections is worth to evaluate especially when bi-modulus behaviour is markedly relevant. This fact is more notable in Figure 7, which shows for the same reference beam of Figure 6, the decrease in absolute deflections at midspan for coefficient  $0 \leq n \leq 1$ .

Also, while the effects on deflections might be looked at as only marginally relevant for the practice of structural design, the corresponding effects on stress and position of neutral axis are more pronounced. The depth of cross section subjected to traction passes from half the height, i.e.,  $h$ , for  $n = 1$  to around 82% of the whole section. As a consequence the maximum tension stress reached shows more than 38% decrease; as a counterbalancing effect, the compression stress heightens.

### 3.2 Application of the analytical model to experimental results

Application of the analytical model to the experimental campaign reported in Section 2 aims at retrieving an estimation of longitudinal stresses reached during three-point bending tests consistently with the bi-modulus material model. Due to the constitutive model, longitudinal stress is neither equal nor symmetric with respect to the neutral axis, which is shifted from the middle of cross section, see Figure 5(b).

To interpret results of the three-point bending tests, outcomes of uniaxial compression tests are employed, in particular, values of Poisson's coefficient and compression Young's modulus. The average values considered for  $E_c$  and  $\nu_c$  refer to the sub-group of UC-specimens that showed the most clustered response, hence,  $E_c = 1,462$  MPa and  $\nu_c = 0.0391$ . Each TB-specimen was analysed individually considering the maximum force and the associated total displacement of the load application point, i.e., including possible indentation effects, see values collected in Table 1.

**Table 1** Maximum force and the associated displacement of the load application point for three-point bending tests

	<i>TB-1</i>	<i>TB-2</i>	<i>TB-3</i>	<i>TB-4</i>	<i>TB-5</i>	<i>TB-6</i>
$W$ [N]	1,231	1,114	907	1,158	1,063	841
$w_{\text{exp}}$ [mm]	0.546	0.426	0.387	0.419	0.406	0.362

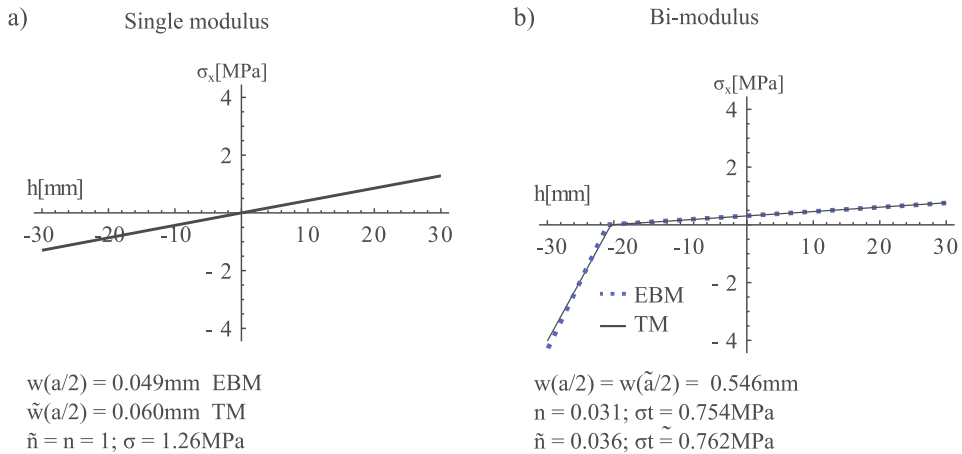
Then, employing equations (7), (26) and (28), value of coefficient  $n$  is retrieved through iterations up to reaching the value of  $z$ -direction displacement in the middle of the

specimen, i.e.,  $w(a/2)$  or  $\tilde{w}(a/2)$ . The value obtained analytically of  $w(a/2)$  or  $\tilde{w}(a/2)$ , and consequently  $n$ , is considered accurate with respect to experimental value, i.e., value of  $\eta$  reported in Table 1, within a 1e-4mm tolerance.

To show the effects of the bi-modulus behaviour on the analysed set of specimens, Figure 8 shows the longitudinal stress distribution at mid-span cross section for specimen TB-1. If the single-modulus assumption is considered, i.e.,  $n = 1$ , then, estimations of deflections at midspan differs between the EBM and TM, Figure 8(a), but stress distribution and value coincide. Assuming a bi-modulus behaviour, Figure 8(b), and imposing that deflection estimation coincides with recorded value, i.e.,  $\tilde{w}(a/2) = w(a/2) = w_{exp}$ , return an asymmetrical stress distribution and neutral axis position since  $E_c \neq E_t$ . Estimations of EBM and TM differs in terms of stress and neutral axis position,  $n \neq \tilde{n}$ , and are represented respectively with dashed lines and continuous black lines.

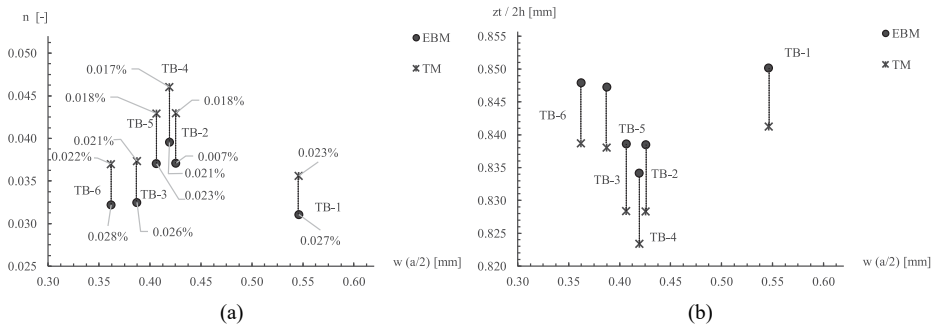
In Table 2, the results of the estimations carried out according to the single- and bi-modulus models are reported. For the single-modulus model, i.e., that employed currently to interpret all the three-point bending tests, the stress reached at peak load is on the average  $\sigma = 1.073$  MPa, that is 42% of the average compressive strength,  $\sigma_c = 2.547$  MPa, and more than three times the average value of indirect tension strength,  $\sigma_{it} = 0.29$  MPa.

**Figure 8** For specimen TB-1, subjected to a maximum point force  $W = 1,231$  N, corresponding to mid span deflection,  $w_{exp} = 0.546$  mm, stress distribution along height assuming, (a) single modulus behaviour which provides a symmetrical distribution and different values of deflection for EBM and TM assuming  $E = 1,634$  MPa (b) bi-modulus behaviour which provides an asymmetrical distribution of stress and the deflection value recorded during tests (see online version for colours)



If instead the bi-modulus model is employed, much more reasonable predictions can be carried out in terms of maximum tension stress reached at the most stretched fibre. Values are on the average lower for both EBM and TM, and more realistic. For EBM, average tensile stress estimated is  $\sigma_t = 0.653$  MPa, which is 25.6% of the compressive strength and nearly two times the recorded values of stress reached during the indirect tension tests. Similar thresholds are attained for the TM.

**Figure 9** For the EBM and TM, (a) value obtained for the coefficient  $n$  plotted over the corresponding mid span deflection,  $w(a/2)$ <sup>1</sup> (b) depth of the stretched part of the cross section, normalised to the height plotted over the midspan deflection,  $w(a/2)$ , found analytically<sup>2</sup>



Notes: <sup>1</sup>for each pointer the relative error with respect to experimental outcome of each deflection value found through the analytical model is indicated.  
<sup>2</sup>vertical dotted lines highlight the difference between estimations of the EBM and TM.

**Table 2** Results of the analytical evaluations for the single- and bi-modulus models interpreting stress distribution of tested rammed earth specimens TB-i, considered as a beam under a point force with cross section 60 mm × 60 mm and free length 150 mm;  $E_c = 1,462$  MPa and  $\nu_c = 0.0391$ , as deduced from uniaxial compression tests

ID	Single modulus		Bi-modulus				
	$\sigma$	$n$	EBM		TM		
			$\sigma_t$	$z_t$	$\tilde{n}$	$\tilde{\sigma}_t$	$\tilde{z}_t$
TB-1	1.260	0.031	0.754	51.01	0.036	0.762	50.47
TB-2	1.135	0.037	0.692	50.31	0.043	0.700	49.70
TB-3	0.923	0.032	0.558	50.84	0.037	0.564	50.28
TB-4	1.183	0.040	0.723	50.05	0.046	0.733	49.40
TB-5	1.081	0.037	0.660	50.32	0.043	0.668	49.70
TB-6	0.854	0.032	0.517	50.87	0.037	0.522	50.32
Av	1.073	0.035	0.651	50.56	0.040	0.658	49.98
CoV	0.133	0.090	0.132	0.007	0.095	0.132	0.008

Notes: Values reported in the table are  $\sigma_t$ , estimated tension stress at the most stretched fibre;  $z_t$  depth of neutral axis evaluated as the positive distance from the most stretched edge; the superscript  $\tilde{\cdot}$ , refers to values for TM.

As a result of the asymmetric stress distribution, the estimation for the Young’s modulus in tension takes values ranging 3.6–4.0% of the compression modulus. Figure 9(a), shows the evaluations provided by the two models in terms of the  $n$  and  $\tilde{n}$  coefficients. For each pointer, the relative error on the estimation of the midspan deflection provided by TM and EBM with reference to the experimental value recorded,  $w_{exp}$ , is reported, the two series are effectively aligned and each couple of pointers represents a tested specimen. The vertical distance between markers of the EBM and TM series highlights

the difference in estimations of Young's modulus in tension, which is, for the EBM, 10% lower of the TM, on the average, cf. Table 2. As a result of the  $n$  and  $\bar{n}$  coefficients values, most of the cross section is subjected to tensile stress, since the neutral axis places at around the upper sixth of the cross section, i.e., roughly at 50 mm compared to a 60 mm-height section. Concerning this, Figure 9(b), shows for each specimen, the depth of the stretched part of the cross section normalised to the total height of the specimen plotted over the deflection value. The stretched depth ranges 82%–85% of the cross section. Comparing the two bi-modulus models, it is seen that for the EBM, stress and coefficient  $n$  are slightly lower for all the specimens, consequently, neutral axis is deeper if compared to the predictions of the TM beam.

The proposed approach was implemented in a Python module for automated determination of the elastic modulus in tension, the compressive and tensile stress for the bimodular beam model of Euler-Bernoulli and of Timoshenko, using the experimental data obtained through three points bending test (load and deflection) and compression test (elastic modulus in compression). The implementation will be documented and made available on <https://github.com> to promote reuse for correct mechanical interpretation of brittle materials, such as mortar, concrete and rammed earth.

#### 4 Conclusions

This paper presents the results of an experimental campaign exploited to provide more robust interpretation of the three-point bending test. Tests on rammed earth specimens were carried out to accurately evaluate the most relevant mechanical properties. From uniaxial compression tests, Young's modulus, Poisson's coefficient and compressive strength are deduced; indirect tension tests and three point bending tests are also employed to complete the characterisation.

Stemming from the consideration of rammed earth as a material that shows two different Young's moduli, for tension and compression, the equilibrium problem of a bent beam under a point force is stated and solved assuming both standard Euler-Bernoulli and Timoshenko beam models.

For a reference case, it is shown that the contribution of shear on deflection increases when the modulus in tension is noticeably lower than that in compression, which is the case of brittle materials, such as concrete and rammed earth. It is shown that the contribution of shearing on deflections is worth considering when the bi-modulus behaviour is markedly relevant. Although the effects of shear might be considered only marginally relevant on deflection values for design purposes, in these cases, i.e., brittle materials, the neutral axis position defines a much wider area of the cross section subject to tension. As a result, the most stretched edge reaches values of tensile stress remarkably lower than those estimated by the standard single modulus Euler-Bernoulli beam.

Solution in terms of displacements is then employed to interpret outcomes of the experimental campaign. Based on the Young's modulus in compression determined on prismatic specimens, it is possible to interpret the three-point bending tests in a sounder way estimating the tension stress, the coefficient relating the two modulus and the depth of the neutral axis. The analytical estimations return values of the tensile stress much more realistic if compared to the outcomes of indirect tensile stress tests.

Results show that earthen materials can exhibit a remarkably low tensile Young's modulus; in the analysed cases, values range around 4% of the modulus in compression evaluated during tests. For the straight applicability and clarity, the model presented can be considered suitable either to analyse future experimental campaigns and to interpret already existing data.

## References

- Ambartsumyan, S. (1965) 'The axisymmetric problem of circular cylindrical shell made of materials with different stiffness in tension and compression', *Izvestiya Akademiyi Nauk SSSR, Mekhanika*, Vol. 4, pp.77–85.
- Azil, C., Djebri, B., Fratini, F., Misseri, G. and Rovero, L. (2020) 'Desert rose stone constructions covered with domes in the Souf Region (Algeria)', *International Journal of Architectural Heritage*, pp.1–20 [online] <https://doi.org/10.1080/15583058.2020.1813353>.
- Bert, C. (1977) 'Models for fibrous composites with different properties in tension and compression', *Journal of Engineering Materials and Technology*, Vol. 99, No. 4, pp.344–349.
- Blondet, M. and Aguilar, R. (2007) 'Seismic protection of earthen buildings', in *International Symposium on Earthen Structures*, Indian Institute of Science, Bangalore, pp.22–24.
- Blondet, M., Vargas, J. and Tarque, N. (2008) 'Available low-cost technologies to improve the seismic performance of earthen houses in developing countries', in *Proceedings, 14th World Conference on Earthquake Engineering*, Citeseer.
- Blondet, M., Vargas, J., Tarque, N. and Iwaki, C. (2011) 'Seismic resistant earthen construction: the contemporary experience at the Pontificia Universidad Católica del Perú', *Informes de la Construcción*, Vol. 63, No. 523, pp.41–50.
- Blondet, M., Tarque, N., Vargas, J. and Vargas, H. (2019) 'Evaluation of a rope mesh reinforcement system for adobe dwellings in seismic areas', in *Structural Analysis of Historical Constructions*, pp.405–412, Springer, Cham (CH).
- Boostani, A., Fratini, F., Misseri, G., Rovero, L. and Toniatti, U. (2018) 'A masterpiece of early Islamic architecture: the Noh-Gonbad Mosque in Balkh, Afghanistan', *Journal of Cultural Heritage*, Vol. 32, pp.248–256.
- Boostani, A., Misseri, G., Rovero, L. and Toniatti, U. (2020) 'The consolidation strategy of the Noh Gonbad mosque vestiges in Balkh (Afghanistan)', *Procedia Structural Integrity*, Vol. 29, pp.79–86.
- Bove, A., Misseri, G., Rovero, L. and Toniatti, U. (2016) 'Experimental and numerical analyses on the antiseismic effectiveness of fiber textile for earthen buildings', *J. Mater. Environ. Sci.*, Vol. 7, No. 10, pp.3548–3557.
- Briceño, C., Moreira, S., Noel, M.F., Gonzales, M., Vila-Chã, E. and Aguilar, R. (2019) 'Seismic vulnerability assessment of a 17th century adobe church in the Peruvian Andes', *International Journal of Architectural Heritage*, Vol. 13, No. 1, pp.140–152.
- Cancino, C., Lardinois, S. and Michiels, T. (2014) *Earthen Architecture Initiative Seismic Retrofitting Project: A Bibliography*, Getty Conservation Institute.
- Caporale, A., Parisi, F., Asprone, D., Luciano, R. and Prota, A. (2014a) 'Critical surfaces for adobe masonry: micromechanical approach', *Composites Part B: Engineering*, Vol. 56, pp.790–796.
- Caporale, A., Parisi, F., Asprone, D., Luciano, R. and Prota, A. (2014b) 'Micromechanical analysis of adobe masonry as two-component composite: influence of bond and loading schemes', *Composite Structures*, Vol. 112, pp.254–263.
- Caporale, A., Parisi, F., Asprone, D., Luciano, R. and Prota, A. (2015) 'Comparative micromechanical assessment of adobe and clay brick masonry assemblages based on experimental data sets', *Composite Structures*, Vol. 120, pp.208–220.

- Cid, J., Mazarrón, F.R. and Cañas, I. (2011) 'Las normativas de construcción con tierra en el mundo', *Informes de la Construcción*, Vol. 63, No. 523, pp.159–169.
- de Saint-Venant, B. (1864) *Resume des Lecons Donnees a Ecole des Ponts et Chaussees sur l'Application de la Mecanique a l'Etablissement des Constructions et des Machines*, Dunod, Vol. 1.
- Du, Z. and Guo, X. (2014) 'Variational principles and the related bounding theorems for bi-modulus materials', *Journal of the Mechanics and Physics of Solids*, Vol. 73, pp.183–211.
- Du, Z., Zhang, Y., Zhang, W. and Guo, X. (2016) 'A new computational framework for materials with different mechanical responses in tension and compression and its applications', *International Journal of Solids and Structures*, Vol. 100, pp.54–73.
- EN-1015-11 (2019) *Methods of Test for Mortar for Masonry – Part 11: Determination of Flexural and Compressive Strength of Hardened Mortar*, European Committee for Standardization.
- EN-12390-6 (2009) *Testing Hardened Concrete – Part 6: Tensile Splitting Strength of Test Specimens*, European Committee for Standardization.
- Fabbri, A., Morel, J-C. and Gallipoli, D. (2018) 'Assessing the performance of earth building materials: a review of recent developments', *RILEM Technical Letters*, December, Vol. 3, pp.46–58.
- Fratini, F., Pecchioni, E., Rovero, L. and Tonietti, U. (2011) 'The earth in the architecture of the historical centre of Lamezia Terme (Italy): characterization for restoration', *Applied Clay Science*, Vol. 53, No. 3, pp.509–516.
- Fratini, F., Rescic, S., Riminesi, C., Mattone, M., Rovero, L. and Tonietti, U. (2015) 'The vernacular earthen architecture near Turin (Piedmont, Italy)', in Mileto, C., Vegas, F., García Soriano and Cristini (Eds.): *Earthen Architecture: Past, Present and Future*, pp.145–150, CRC Press, London.
- Gamrani, N., Chaham, K.R., Ibnoussina, M., Fratini, F., Rovero, L., Tonietti, U., Mansori, M., Daoudi, L., Favotto, C. and Youbi, N. (2012) 'The particular 'Rammed Earth' of the Saadian sugar refinery of Chichaoua (XVIIth century, Morocco): mineralogical, chemical and mechanical characteristics', *Environmental Earth Sciences*, Vol. 66, No. 1, pp.129–140.
- He, X-t., Zheng, Z-l., Sun, J-y., Li, Y-m. and Chen, S-l. (2009) 'Convergence analysis of a finite element method based on different moduli in tension and compression', *International Journal of Solids and Structures*, Vol. 46, No. 20, pp.3734–3740.
- He, X-T., Li, W-M., Sun, J-Y. and Wang, Z-X. (2018) 'An elasticity solution of functionally graded beams with different moduli in tension and compression', *Mechanics of Advanced Materials and Structures*, Vol. 25, No. 2, pp.143–154.
- Houben, H. and Guillaud, H. (1994) *Earth Construction. A Comprehensive Guide*, Distributeur Craterre-Eag.
- IAEE (2004) *Guidelines for Earthquake Resistant Non-Engineered Construction*, National Information Center of Earthquake Engineering.
- Illampas, R., Ioannou, I. and Charmpis, D.C. (2014) 'Adobe bricks under compression: experimental investigation and derivation of stress-strain equation', *Construction and Building Materials*, February, Vol. 53, pp.83–90.
- INN (2013) *Instituto Nacional de Normalizacion. NCH 3332. Intervención de Construcciones Patrimoniales de Tierra Cruda – Requisitos del Proyecto Estructural*.
- Janmey, P.A., McCormick, M.E., Rammensee, S., Leight, J.L., Georges, P.C. and MacKintosh, F.C. (2007) 'Negative normal stress in semiflexible biopolymer gels', *Nature Materials*, Vol. 6, No. 1, p.48.
- Jiménez Delgado, M.C. and Guerrero, I.C. (2007) 'The selection of soils for unstabilised earth building: a normative review', *Construction and Building Materials*, February, Vol. 21, No. 2, pp.237–251.

- Jones, R.M. (1977) 'Stress-strain relations for materials with different moduli in tension and compression', *AIAA Journal*, Vol. 15, No. 1, pp.16–23.
- Kanno, Y. (2011) *Nonsmooth Mechanics and Convex Optimization*, CRC Press, Boca Raton, FL.
- Langenbach, R. (2005) 'Performance of the earthen Arg-e-Bam (Bam Citadel) during the 2003 Bam, Iran, earthquake', *Earthquake Spectra*, Vol. 21, No. S1, pp.345–374.
- Liberotti, G., Rovero, L., Stipo, G. and Toniatti, U. (2016) 'Mechanical investigation on adobe samples belonging to the archaeological site of Arslantepe (Malatya, Turkey)', *CIAT2015. Congrès International sur l'Architecture de Terre en Afrique du Nord (Marrakech 2015)*, pp.3656–3666.
- Liu, Y., Xie, Z., Van Humbeeck, J. and Delaey, L. (1998) 'Asymmetry of stress-strain curves under tension and compression for NiTi shape memory alloys', *Acta Materialia*, Vol. 46, No. 12, pp.4325–4338.
- Lourenço, P.B., Ciocci, M.P., Greco, F., Karanikoloudis, G., Cancino, C., Torrealva, D. and Wong, K. (2019) 'Traditional techniques for the rehabilitation and protection of historic earthen structures: the seismic retrofitting project', *International Journal of Architectural Heritage*, Vol. 13, No. 1, pp.15–32.
- Marin, J. (1962) *Mechanical Behavior of Engineering Materials*, Prentice-Hall, Englewood Cliffs, NJ.
- Mattos, H.C., Fremond, M. and Mamiya, E. (1992) 'A simple model of the mechanical behavior of ceramic-like materials', *International Journal of Solids and Structures*, Vol. 29, No. 24, pp.3185–3200.
- Michiels, T.L. (2015) 'Seismic retrofitting techniques for historic adobe buildings', *International Journal of Architectural Heritage*, Vol. 9, No. 8, pp.1059–1068.
- Minke, G. (2005) *Construction Manual for Earthquake-Resistant Houses Built of Earth*, X-Change.
- Misseri, G., Palazzi, C. and Rovero, L. (2020) 'Seismic vulnerability of timber-reinforced earthen structures through standard and non-standard limit analysis', *Engineering Structures*, Vol. 215, p.110663.
- Morel, J.C., Pkla, A. and Walker, P. (2007) 'Compressive strength testing of compressed earth blocks', *Construction and Building Materials*, February, Vol. 21, pp.303–309.
- NMAC (1982) *New Mexico State Building Code, Section 2405 – Amendment*.
- NSZ (1998) *Engineering Design of Earth Buildings. NSZ 4297*, Standards, New Zealand.
- Ortega, J., Vasconcelos, G., Rodrigues, H., Correia, M. and Lourenço, P.B. (2017) 'Traditional earthquake resistant techniques for vernacular architecture and local seismic cultures: a literature review', *Journal of Cultural Heritage*, Vol. 27, pp.181–196.
- Ortega, J., Vasconcelos, G., Rodrigues, H. and Correia, M. (2018) 'Assessment of the efficiency of traditional earthquake resistant techniques for vernacular architecture', *Engineering Structures*, Vol. 173, pp.1–27.
- Parisi, F., Asprone, D., Fenu, L. and Prota, A. (2015) 'Experimental characterization of Italian composite adobe bricks reinforced with straw fibers', *Composite Structures*, Vol. 122, pp.300–307.
- Parisi, F., Balestrieri, C. and Varum, H. (2019) 'Nonlinear finite element model for traditional adobe masonry', *Construction and Building Materials*, Vol. 223, pp.450–462.
- Portugal, H. and Tarque, N. (2019) 'Non-linear modelling of a geomesh-reinforced Earthen wall subjected to dynamic loading', in *Structural Analysis of Historical Constructions*, pp.1108–1116, Springer, Cham (CH).
- Reddy, J.N. (2004) *Mechanics of Laminated Composite Plates and Shells: Theory and Analysis*, CRC Press, Boca Raton, FL, USA.
- Reddy, J.N. (2006) *Theory and Analysis of Elastic Plates and Shells*, CRC Press, Boca Raton, FL, USA.

- Rodríguez-Mariscal, J.D., Solís, M. and Cifuentes, H. (2018) 'Methodological issues for the mechanical characterization of unfired earth bricks', *Construction and Building Materials*, Vol. 175, pp.804–814.
- Rosakis, P., Notbohm, J. and Ravichandran, G. (2015) 'A model for compression-weakening materials and the elastic fields due to contractile cells', *Journal of the Mechanics and Physics of Solids*, Vol. 85, pp.16–32.
- Rovero, L. and Tonietti, U. (2012) 'Structural behaviour of earthen corbelled domes in the Aleppo region', *Materials and structures*, Vol. 45, No. 1, pp.171–184.
- Rovero, L. and Tonietti, U. (2014) 'A modified corbelling theory for domes with horizontal layers', *Construction and Building Materials*, Vol. 50, pp.50–61.
- Rovero, L., Tonietti, U., Fratini, F. and Rescic, S. (2009) 'The salt architecture in Siwa Oasis – Egypt (XII–XX centuries)', *Construction and Building Materials*, Vol. 23, No. 7, pp.2492–2503.
- Rovero, L., Galassi, S. and Misseri, G. (2020) 'Experimental and analytical investigation of bond behavior in glass fiber-reinforced composites based on gypsum and cement matrices', *Composites Part B: Engineering*, Vol. 194, p.108051.
- Silveira, D., Varum, H. and Costa, A. (2013) 'Influence of the testing procedures in the mechanical characterization of adobe bricks', *Construction and Building Materials*, March, Vol. 40, pp.719–728.
- Sun, J-y., Zhu, H-q., Qin, S-h., Yang, D-l. and He, X-t. (2010) 'A review on the research of mechanical problems with different moduli in tension and compression', *Journal of Mechanical Science and Technology*, Vol. 24, No. 9, pp.1845–1854.
- Timoshenko, S.P. and Goodier, J.N. (1930) *Theory of Elasticity*, McGraw-Hill, New York.
- Tran, A. and Bert, C. (1982) 'Bending of thick beams of bimodulus materials', *Computers & Structures*, Vol. 15, No. 6, pp.627–642.
- UNESCO (2017) *World Heritage Earthen Architecture Programme* [online] <https://whc.unesco.org/en/earthen-architecture/> (accessed 7 October 2021).
- Vissilia, A-M. and Villi, M. (2010) 'Adobe and timber ties as main construction materials for an historic Greek dwelling', *International Journal of Architectural Heritage*, Vol. 4, No. 4, pp.295–319.
- Yao, W.Y. and Ye, Z.M. (2004a) 'Analytical solution for bending beam subject to lateral force with different modulus', *Applied Mathematics and Mechanics*, Vol. 25, No. 10, pp.1107–1117.
- Yao, W.Y. and Ye, Z.M. (2004b) 'Analytical solution of bending-compression column using different tension-compression modulus', *Applied Mathematics and Mechanics*, Vol. 25, No. 9, pp.983–993.
- Zhang, H., Zhang, L. and Gao, Q. (2011) 'An efficient computational method for mechanical analysis of bimodular structures based on parametric variational principle', *Computers & Structures*, Vol. 89, Nos. 23–24, pp.2352–2360.
- Zhang, L., Zhang, H., Wu, J. and Yan, B. (2016) 'A stabilized complementarity formulation for nonlinear analysis of 3D bimodular materials', *Acta Mechanica Sinica*, Vol. 32, No. 3, pp.481–490.